ChemPubSoc Europe

DOI: 10.1002/batt.201900053

BATTERIES & SUPERCAPS
Articles

Facile, Solvent-Free Preparation of High Density, High Mass Loading Sulfur Cathodes Enabled by Dry-Pressable Holey Graphene Scaffolds

Yi Lin,*[a] Kobi J. Jones,[b] Louisa C. Greenburg,[b] Jae-Woo Kim,[a] Liangbing Hu,[c] and John W. Connell*[d]

For lithium-sulfur (Li–S) batteries to be practically applicable in large scale, high mass loading and high S content are required for the sulfur (S) cathodes. Most reported S cathode preparation procedures, such as melt infiltration of S into carbon scaffolds followed by conventional solvent-based slurry casting, are time-consuming, costly, and lack control with respect to the electrode composition and quality. Here we report the use of a facile room-temperature procedure that is especially useful in the preparation of high density, high mass loading S cathodes with convenient control of S content and electrode architecture. The solvent-free and binder-free procedure is enabled by the use of holey graphene (hG) as a unique dry-pressable electrode scaffold host to effectively encapsulate S in the conductive matrix. The entire process can be completed within just a few minutes at room temperature, in comparison to much longer time required for most other methods. With effective S utilization, the high mass loadings and high densities of the dry-pressed hG-hosted S cathodes result in excellent areal (up to 20 mAh/cm^2) and volumetric performance (1787 mAh/cm^3 is the highest reported to date), respectively. The hG-enabled dry-press method therefore offers an attractive processing option for S composite cathode fabrication toward practical applications.

1. Introduction

There has been increasing demand for high energy density batteries for electrical applications, especially those for transportation such as electric cars and aircrafts.[1] With theoretical capacity of 1675 mAh/g$_S$ and energy density of 2600 Wh/kg$_S$, lithium sulfur (Li–S) batteries are considered one of the most promising candidates to replace current state-of-the-art lithium ion batteries which have nearly reached the limit of the theoretical energy density.[2–6]

In the typical Li–S battery chemistry, sulfur (S) at the cathode during discharge is first reduced into polysulfides of various chain lengths (e.g., Li_2S_x, x = 2–8) and eventually Li_2S. In the subsequent charge reaction, the complex electrochemical system takes the reverse course to convert the reduction products back to S. Because both S and Li_2S are insulating and insoluble in the electrolyte, a conductive host is often needed to effectively encapsulate the sulfur species in the cathode architecture to facilitate the electrochemical reactions.[7] Among various types of conductive hosts, carbon nanomaterials, such as carbon nanotubes[8–10] and graphene,[11–13] have been shown to be excellent platforms because of their electrical conductivity, high surface area, low mass, mechanical robustness, and chemical stability. With some modifications such as heteroatomic doping[14,15] or incorporation of polymeric or inorganic additives,[16,17] these carbon nanomaterials can also help significantly reduce polysulfide dissolution and shuttling that are detrimental to the cyclability of Li–S batteries.[18]

It has been recently emphasized that, for Li–S batteries to be practically meaningful, a number of cell parameters must be met.[6,19–22] For example, according to Manthiram and coworkers,[22] an ideal device shall simultaneously consist of (1) high S mass loading (> 13 mg/cm^2), (2) high S content (> 70%), and (3) low electrolyte/S (E/S) ratio (< 4 μL/mg$_S$), while (4) achieving high capacities (> 80% S utilization or > 1340 mAh/g$_S$) with (5) substantial cyclability (> 200 cycles with at least 70% capacity retention). Many researchers over the past five years or so have focused on addressing one or more of these aspects, but it remains elusive for existing Li–S battery designs to simultaneously meet all requirements and also be scalable into large cells.

The conventional method to fabricate a lithium ion battery cathode is to first mix the active material with up to 20 wt% of conductive carbon and binder additives using a polar solvent, often a high boiling point organic solvent such as N-methyl-2-pyrrolidone (NMP), to form a slurry. The slurry is then cast onto

[a] Dr. Y. Lin, Dr. J.-W. Kim
National Institute of Aerospace
100 Exploration Way, Hampton, VA 23666, USA
E-mail: yi.lin-1@nasa.gov
[b] K. J. Jones, L. C. Greenburg
NASA Interns, Fellows, and Scholars (NIFS) Program
NASA Langley Research Center
Hampton, VA 23681, USA
[c] Prof. L. Hu
Department of Materials Science and Engineering
University of Maryland
College Park, MD 20740, USA
[d] Dr. J. W. Connell
Advanced Materials and Processing Branch
NASA Langley Research Center
Mail Stop 226, Hampton, VA 23681, USA
E-mail: john.w.connell@nasa.gov

Supporting information for this article is available on the WWW under https://doi.org/10.1002/batt.201900053

a current collector such as aluminum (Al) foil, followed by evaporating the solvent.[23] This method has also been widely applied in S cathode fabrication.[24] Generally, such electrode fabrication approaches require a lengthy process for homogeneous slurry preparation and solvent removal, especially in the case of NMP which has a high boiling point and difficult to fully remove. In addition, other concerns relevant to organic solvents include toxicity, containment, and disposal, all of which add costs to the process. For Li–S batteries, other than a few exceptions,[25–28] most reported S cathodes from slurry casting were of low S mass loadings (<2 mg/cm^2) and therefore lack of practicality, despite impressive unit cathode performance. Further, multiple fabrication-related problems such as non-uniform coatings and cracks were encountered, as well as formidable challenges toward achieving the requisite high S content and low E/S ratio.[22,24] An alternative approach that was recently proposed for high mass loading S cathodes is to first prepare a nanocarbon-based scaffold disc in the form of either a membrane or a foam, followed by S infiltration in the melt or via sublimation.[6] However, the preparation of the scaffold discs are also usually solvent-based, time-consuming, and difficult to scale up, with challenges in controlling the S content and distribution within the thick scaffold architecture during infiltration.

We and others recently discovered several methods to prepare holey graphene (hG), which is a structural derivative of graphene that exhibits arrays of nanometer-sized holes distributed across the lateral nanosheet surface.[29–37] hG has recently emerged to be an advanced alternative to intact graphene as an electrode material for electrochemical energy storage applications because the through-thickness holes facilitate ion transport across the nanosheet planes, a feature that is not attainable with intact graphene.[30,33–36] More recently, we discovered another outstanding attribute of hG in that the as-produced lightweight powder, without the use of any solvent or binder material, can be directly compression molded into dense, porous, yet robust articles or architectures of arbitrary shapes.[38] This characteristic is enabled by the presence of holes through the graphene sheets and is unique to hG but not available from intact graphene or any other carbon allotropes. With the dry compressibility, high mass loading neat hG electrodes were conveniently fabricated for applications such as supercapacitors[39] and lithium-oxygen (Li—O_2) batteries.[40,41] The high electrode mass loading coupled with the facile through-plane ion transport enabled ultrahigh areal capacity in both cases. For supercapacitors, 1.25 F/cm^2 was achieved with an ultrahigh 30 mg/cm^2 material loading.[39] For Li—O_2 batteries, 40 mAh/cm^2 was obtained with 10 mg/cm^2 hG in the air cathode.[40]

Here we report the preparation of high mass loading S composite cathodes with hG as a host matrix and conductive scaffold using the facile, versatile, and scalable dry compression fabrication method. The entire process is completed within minutes, providing significant advantages especially in terms of fabrication time and cost over the widely adopted conventional slurry approach and other alternative methods reported in the literature. The dry compression approach allows the convenient tuning and achievement of the desired S mass loading, S content, and electrode composition architecture. Such S composite cathodes from the extremely facile process exhibited excellent S utilization with high gravimetric, areal, and volumetric performances.

2. Results and Discussion

2.1. Preparation and Characterization of hG/S Composite Cathodes

The hG-hosted S (hG/S) composite cathodes were prepared in a facile solvent-free and binder-free procedure, as illustrated in Figure 1. Briefly, hG powder was first mixed with S powder, and the solid mixture was directly loaded in a compression die and pressed into the final electrode shape. In a specific example, lightweight hG powder (tap density ~7.6 mg/cm^3) and dense S powder (tap density ~1.1 g/cm^3) were mixed with a weight ratio of 1:1 (or apparent volume ratio of ~145:1) using a ball-mill. It was observed that long ball-milling time could significantly densify the lightweight hG powder causing it to become less moldable when subjected to dry-press. It is known that extensive ball-milling, often used in electrode material mixing, may cause physical damage to carbon nanostructures.[42] Interestingly, ball-mill mixing for only 10 s was very effective as the mixture of the two powders of distinctively different tap densities appeared visually homogeneous, with a final tap density of ~38 mg/cm^3 (Figure 1 and Figure S1). This mixture was then readily compressed to form a hG/S composite disc containing 50 wt% S (hG/S-50%) using a cylindrical die (d ~1.485 cm) at a hydraulic pressure of 200 MPa. The density of the hG/S-50% disc was 1.25 g/cm^3, while a neat hG disc with no S under similar preparation conditions exhibited a lower density of 0.92 g/cm^3. Therefore, considering the neat S density of 2.07 g/cm^3,[2] the volume ratio of hG:S in the final formed disc was thus calculated to be ~7:3 (v/v). Such high density values for the S composite discs are essential for their excellent volumetric performance, as discussed in later sections. Despite the high density, the hG/S composite disc retained most of the porosity from the hG material itself, which was shown to exhibit rich micro- and mesoscale pore characteristics.[34] More specifically, the nitrogen (N_2) adsorption-desorption isotherm of the hG/S-50% disc exhibited similar Type-IV shape to that of a neat hG disc (Figure S2a) and similar pore size distribution (Figure S2b), indicating retained mesoporous characteristics. In addition, the Brunauer–Emmett–Teller (BET) surface area for the hG/S-50% disc estimated from the isotherm was as high as 148 m^2/g, in comparison to 256 m^2/g for a neat hG disc. Considering half of the weight of the composite disc is attributed to S, the micro- and meso-porosity afforded mainly by hG and beneficial for electrochemical ion diffusion remained largely unchanged in the dry-pressed hG/S composite disc.

The room temperature solvent-free mixing and compression processes for electrode fabrication did not induce any structural changes to the S. As shown in the X-ray diffraction

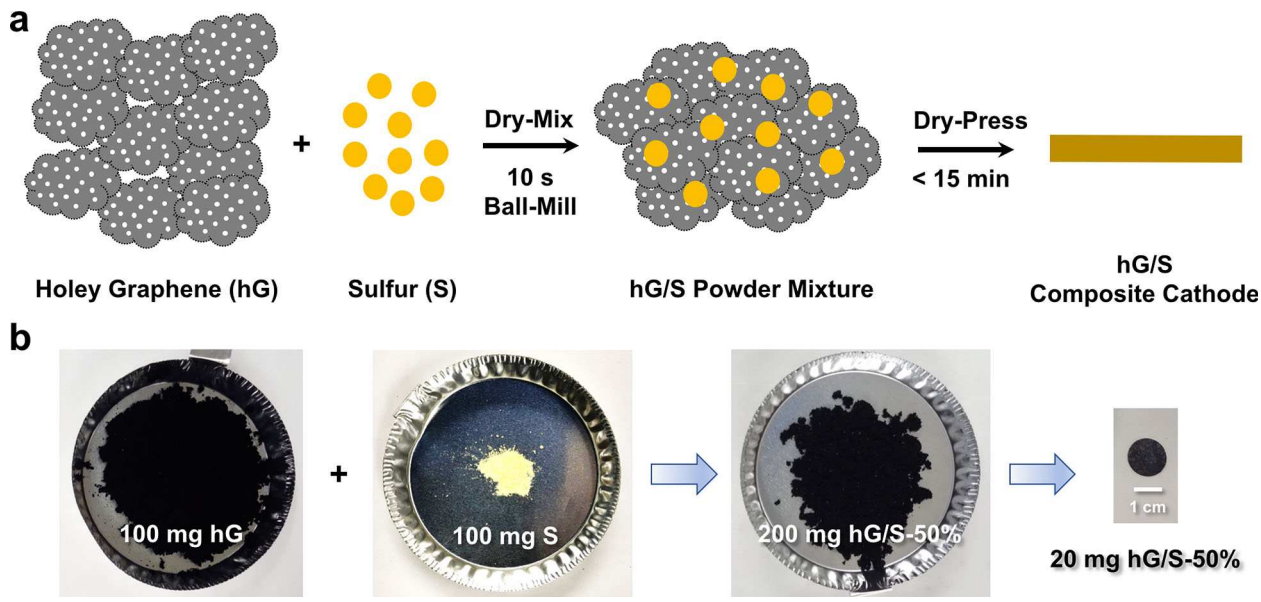

Figure 1. a) The facile solvent-free process for the preparation of hG/S composite cathodes from hG and S powder. b) Photographs (in the same scale; scale bar = 1 cm) of 100 mg hG powder, 100 mg S powder, 200 mg hG/S powder mixture (1 : 1, w/w; "hG/S-50%") and a 20-mg formed composite disc electrode of the same composition (diameter ~ 1.49 cm).

(XRD) patterns in Figure 2a, all peaks from the neat S powder were still present in both the as-mixed hG/S powder and the final formed disc. The broad peak centered at ~ 26° for both the mixture powder and the disc could be readily attributed to the weak (002) graphitic signature from the few-layered graphene structure of hG.[33] The intensity of this peak was much more prominent for the hG/S-50% disc than the mixture powder. This suggests that, despite the presence of 50 wt% S in the disc, the vertical compression molding resulted in excellent lateral alignment and stacking of the two-dimensional hG sheets.

The morphology and microscopic distribution of S within a hG/S-50% disc with a total mass loading (m_A) of ~ 11 mg/cm^2 or a S mass loading ($m_{A\text{-}S}$) of 5.5 mg/cm^2 was evaluated with scanning electron microscopy (SEM) coupled with energy-dispersive X-ray spectroscopy (EDS) mapping of the disc cross-section. As shown in Figure 2b and Figure S3, layered sheet-like structures were found in the cross-section of the hG/S-50% disc, consistent with the XRD results that suggested the alignment and stacking of the hG sheets. With a dominating volumetric fraction (~ 70%), the morphology of the stacked sheets is similar to that found in neat hG discs,[38] except for a smoother cross-sectional appearance likely due to the presence of S with a densified morphology. Impressively, elemental S was found to be well distributed across the entire disc thickness of ~ 90 μm (Figure 2c), indicating the surprising effectiveness of the ball-mill mixing with such short duration (10 s).

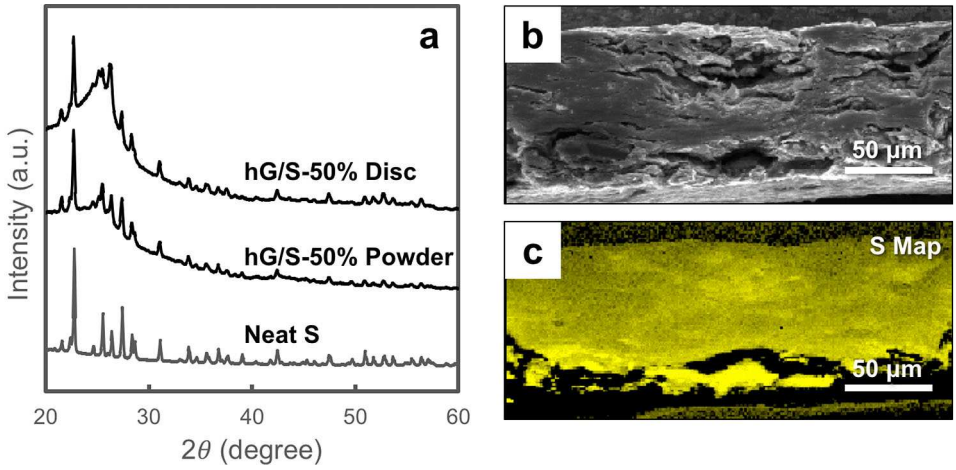

Figure 2. a) XRD patterns of hG/S-50% powder mixture and disc in comparison to that of neat S. b) A typical SEM image and c) the corresponding S map from EDS of the cross-section of a hG/S-50% disc (S mass loading $m_{A\text{-}S}$ ~ 5.5 mg/cm^2).

2.2. Electrochemical Performance of hG/S Composite Cathodes

Despite the insulating S (conductivity on the order of 5×10^{-28} S/cm),[2] the surface conductivity (λ) of the hG/S-50% disc was measured to be as high as 102 S/cm (vs. 324 S/cm for the neat hG disc), thus suitable to be directly used as a cathode for Li–S batteries. Consistently, a typical electrochemical impedance spectrum (EIS) for a Li–S battery with a high S mass loading hG/S-50% cathode (20 mg total, S mass loading $m_{A\text{-}S}\sim$ 6 mg/cm^2) (Figure S4) exhibited an internal resistance (x-axis intercept at high frequency) of ~8 Ω and a low charge transfer resistance (the size of the semicircle) of ~80 Ω. The cyclic voltammogram (CV) curve from the same battery (scan rate = 0.01 mV/s) is shown in Figure 3a. In the cathodic scan, two main reduction peaks at 2.34 and 2.05 V correspond to the formation of long-chain and short-chain polysulfides, respectively. The well-defined shoulder peak at 1.95 V is readily assigned to the final formation of Li_2S. The anodic scan exhibited a rather broad oxidation feature, which could be assigned to the reverse reactions of all reduction events, i.e., the oxidation of Li_2S into polysulfides and then further back to S. The CV behavior of the dry-pressed hG/S composite cathode is similar to what has been commonly observed for various nanocarbon-hosted S composite cathodes fabricated using the conventional slurry-casting method or other approaches.[2–6]

The typical discharge and charge performance were measured for a Li–S battery with a hG/S-50% cathode ($m_{A\text{-}S}\sim$ 6 mg/cm^2) in the voltage range of 1.8–2.6 V. The cycling sequence was conducted at current densities in the order of 0.5, 1, 1.5, 2, and back at 0.5 mA/cm^2, respectively, for 5 cycles each. The first cycles at each current density are compared in Figure 3b. The battery exhibited excellent initial S utilization efficiency, with the first discharge capacity in terms of S weight as high as 1429 mAh/g$_S$ (or 8.2 mAh/cm^2; 85% S utilization) at 0.5 mA/cm^2. Because of the high cathode and S packing densities (1.25 g/cm^3 and 0.63 g$_S$/cm^3, respectively), the volumetric capacity was calculated to be 967 mAh/cm^3. The first discharge curve exhibited two distinct plateaus at ~2.34 and ~2.08 V, which could be readily attributed to the stepwise reduction of S into polysulfides with different chain lengths according to the well-established behavior.[2] The steep voltage drop at the end of discharge indicates the full conversion into Li_2S. The subsequent charge curve exhibited a steady increase in slope at 2.30–2.35 V and the subsequent short plateau at ~2.37 V, which corresponds to the gradual oxidation of Li_2S to polysulfides of increasing chain lengths. The abrupt voltage increase at the end of charge indicates the final conversion back to S. These reduction and oxidation events are consistent with what was observed from CV (Figure 3a) and similar to those of various S cathodes reported in the literature.[2–6] Overall, the results indicate that the hG/S composite cathode from the facile solvent-free mix-and-press fabrication approach

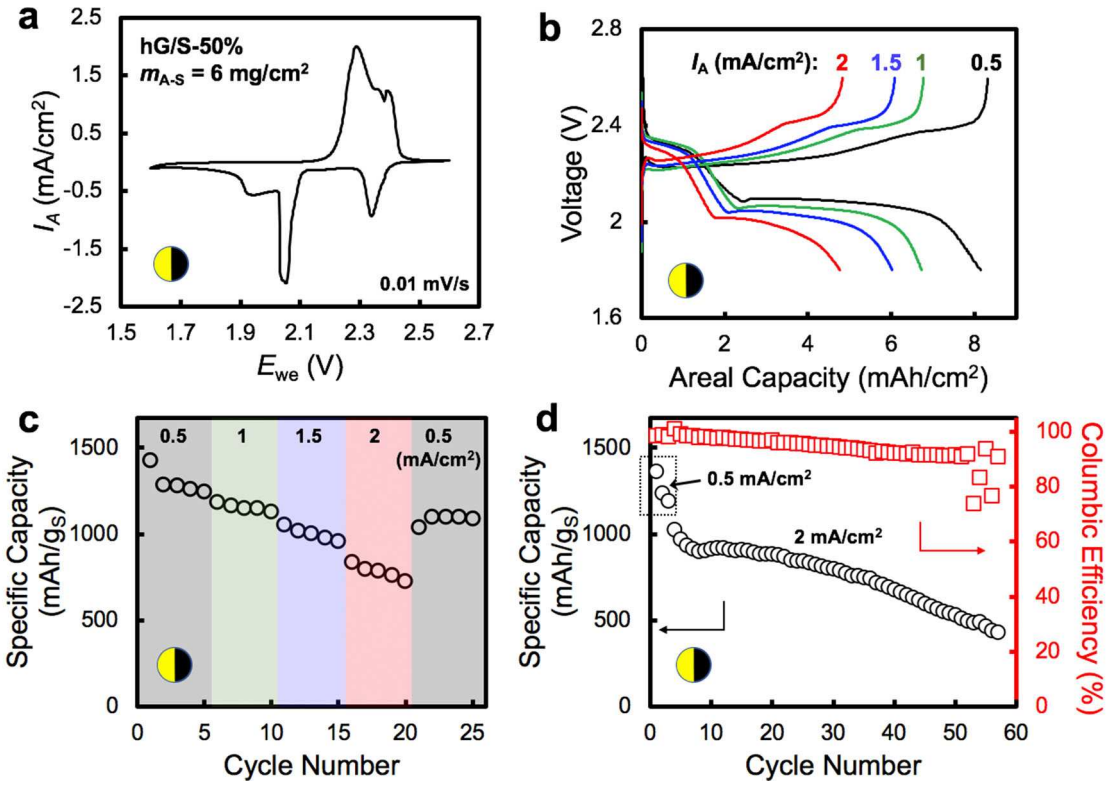

Figure 3. Electrochemical performance of Li–S batteries with hG/S-50% cathodes ($m_{A\text{-}S}$ = 6 mg/cm^2): a) CV (scan rate = 0.01 mV/s); b) discharge-charge properties at various current densities (from right to left: 0.5, 1, 1.5, 2 mA/cm^2) taken from the first cycle of each current density in the cycling experiment depicted in (c); c) change of specific capacity values over cycling at different current densities; d) specific capacity and Columbic efficiency values over cycling at 2 mA/cm^2 (first 3 cycles were run at 0.5 mA/cm^2). The inset symbol in each of the panels indicate the 50% S content in the cathode (yellow: S; black: hG).

was sufficient to allow the S phase to achieve effective electrochemical contact with the conductive hG scaffold. Thus, most of the S, through the contact with the surrounding hG nanosheets as the scaffold host, could be electrochemically reduced into polysulfides and eventually Li_2S, which was then electrochemically converted back to S, both with high efficiency.

As expected, the discharge capacity decreased with the increase of current density, but still maintained a high value. For example, the second discharge capacity values were 1288, 1163, 1021, and 795 mAh/g_S at 0.5, 1, 1.5, and 2 mA/cm^2, respectively. When the current density was changed back to 0.5 mA/cm^2, the discharge capacity recovered to ~1090 mAh/g_S (Figure 3c). A fresh battery with a similar hG/S-50% cathode was run for over 50 cycles at a high current density of 2 mA/cm^2 (run at 0.5 mA/cm^2 for the first 3 cycles for activation) with capacity still retained at 534 mAh/g_S at cycle 50 (Figure 3d). The Columbic efficiency values of the 1st, 10th, and 50th cycles were 98.6, 97.8, and 91.4%, respectively.

Post-mortem analyses on the hG/S-50% composite cathodes were conducted after first discharge, first charge, and prolonged cycling (>50 cycles). All cathode discs largely retained their structural integrity when detached from the separator, with the one after prolonged cycling being the most brittle when handling. For microscopy analysis, it is preferable to rinse the cathode materials with a solvent such as 1,2-dimethoxyethane (DME) to remove excess electrolyte. While the discs after first discharge and charge swelled but still retained their shapes, the cycled disc disintegrated during rinse. Therefore, the latter was directly analyzed without the rinsing step. Low magnification SEM images (Figure S5a, c, e) show that the cathode discs after the first discharge and charge remained rather dense, less but still comparable to the morphology of the as-prepared composite disc from the dry compression process (Figure 2b). The cycled disc, however, was much more porous even in the absence of the solvent rinse.

XRD patterns of the cathodes show (Figure S6a) that the peaks associated with pure S from the starting hG/S-50% disc diminished after the first discharge. Some of the remaining peaks could be assigned to typical Li_2S patterns (PDF# 23-369); others are tentatively attributed to incomplete discharge products such as short-chain polysulfide Li salts. High magnification SEM (Figure S5b, d, f) revealed that the hG sheet surfaces were covered with nanoplatelet species with dimensions <200 nm, which can be readily attributed to the electrochemically formed discharge products identified in XRD. Upon charge, Li_2S peaks disappeared and the S patterns re-emerged in the reverse electrochemical reaction. The S nanocrystals formed from the charge reaction were of nanorod morphology, ~30–60 nm in diameter and ~100–250 nm in length, covering the surfaces of the hG sheets. After prolonged cycling, the hG sheets in the cathode remained intact as expected. However, no well-defined structures could be found on hG sheet surfaces. XRD data exhibited broadened S patterns as well as other intermediate polysulfide species and even the presence of Li_2S, suggesting the incomplete electrochemical conversions during prolonged cycling.

The corresponding Li anodes from the above cells were also carefully analyzed. As shown in Figure S7, the Li chip after the first discharge lost its reflective metallic surface as expected, since Li was partially stripped off during the electrochemical reaction. The corresponding SEM image (Figure S8b) shows a slightly roughened surface, in comparison to the flat morphology of a fresh Li chip (Figure S8a). After the first charge, the re-deposited Li formed islands with dimensions >100 μm (Figure S8c). However, after prolonged cycling, the dark-colored Li anode surface (Figure S7) became much roughened, with grain sizes of only a few μm or less (Figure S8d). XRD data of these Li anodes all exhibited typical Li crystalline patterns at 36.1° (110), 51.9° (200), and 65.2° (211) (Figure S6b). Notably, the relative intensity of the anode after prolonged cycling became much weaker, indicating degraded structure, consistent with the above microscopic findings.

Overall, the postmortem analyses of the hG/S composite cathodes and Li anodes suggest that the electrochemical reactions in the initial cycles were well defined, consistent with the high cell capacity and S utilization. However, prolonged cycling induced severe morphological degradation of both composite cathode and Li anode, with the electrochemical reaction during each later cycles becoming increasingly incomplete. These results suggest that much improvement needs to be made toward cathode integrity and Li anode protection in order to improve the overall cyclability. More discussions are provided in Section 2.4 below.

2.3. Increasing S Content and Mass Loading in hG/S Composite Cathodes

As stated in the Introduction, it is desirable to increase S content and mass loading in the cathode to improve the total electrode and device gravimetric performance as long as the S utilization efficiency is retained. In the solvent-free electrode fabrication process reported here, this can be conveniently achieved by adding more S when preparing the solid hG/S powder mixture. For example, a hG/S disc cathode with 80 wt% S (hG/S-80%) was prepared by dry pressing the powder mixture consisting of hG:S = 1:4 (w/w) after 10-s ball-mill mixing. Similar to the hG/S-50% discs, the S crystalline phase in the hG/S-80% specimen was well preserved from XRD (Figure 4a). The S phase was well distributed across the entire electrode cross-section, as seen from SEM/EDS analyses (Figure 4a inset).

The discharge and charge performances of the Li–S batteries with high mass loading, high S content electrodes were measured in the voltage window of 1.4–2.8 V. The first discharge capacity of a hG/S-80% electrode with $m_{A\text{-}S}$ ~9.2 mg/cm^2 (total mass 20 mg; total mass loading m_A ~11.6 mg/cm^2) at 0.5 mA/cm^2 was measured to be 1291 mAh/g_S, suggesting a good S utilization efficiency of 77%. In comparison, under the same testing conditions, a hG/S-50% electrode of the same total mass loading m_A (11.6 mg/cm^2) and thus lower $m_{A\text{-}S}$ (5.8 mg/cm^2) exhibited a somewhat higher specific capacity of 1547 mAh/g_S as expected. However, because of the higher

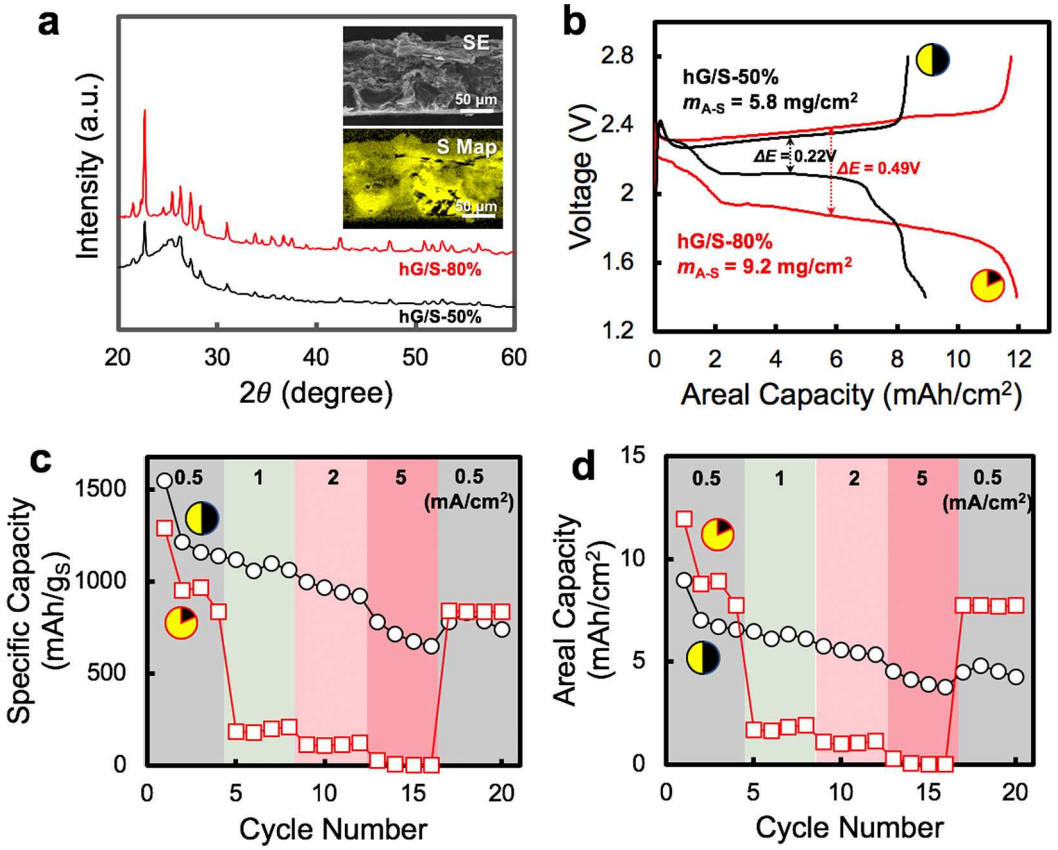

Figure 4. a) XRD pattern of a hG/S-80% composite disc in comparison to that of a hG/S-50% disc. Inset shows the SEM image (top) and the corresponding S map (bottom) of the cross-section of a hG/S-80% disc (total mass 30 mg; m_{A-S} ~ 13.9 mg/cm^2). b) The first cycles of Li–S batteries with hG/S-80% and hG/S-50% cathodes of the same total mass loadings (11.6 mg/cm^2) but different S mass loadings (9.2 vs. 5.8 mg/cm^2) due to different S contents. c) and d) show the rate performances of the same two batteries in terms of specific and areal capacity values, respectively. The cycling experiments were conducted at current densities of 0.5, 1, 2, 5, and 0.5 mA/cm^2, respectively, for 4 cycles each. The inset symbols in each of the panels indicate the S contents in the cathodes (yellow: S; black: hG).

mass loading with higher S content, the areal capacity of the hG/S-80% cathode improved to 11.9 mAh/cm^2, in comparison to 8.9 mAh/cm^2 from the hG/S-50% cathode (Figure 4b). Importantly, the density of the hG/S composite discs increased with S content (~1.7 g/cm^3 for hG/S-80%; see Figure S1; or 1.36 g_S/cm^3). Because of the high density, the volumetric capacity of the cathode was calculated to be as high as 1787 mAh/cm^3, a significant improvement from 967 mAh/cm^3 of the hG/S-50% cathode and among the highest values reported in the literature (Table S1; Figure S9).

As shown in Figure 4b, similar to the hG/S-50% cathode, the first discharge curve of the hG/S-80% cathode also exhibited two plateaus that could be similarly assigned to the stepwise conversion of S into polysulfides of various chain lengths, while the charge curve consisted of a single slope from the reverse oxidation events. Although the charge voltage remained similar, the discharge voltage was noticeably much lower (~1.87 V), resulting in a much increased overpotential (ΔE ~ 0.49 V vs. ~0.22 V for hG/S-50%). Low discharge voltage is undesirable since it leads to low energy density of a battery device, while large overpotential reduces its energy efficiency.[1] The rate performance of hG/S-80% was also much poorer than hG/S-50%, as the former exhibited a significant reduction in specific capacity when the current increased to 1 mA/cm^2 (184 vs. 1120 mAh/g_S for hG/S-50%; Figure 4c), even in terms of areal values (1.7 vs. 6.5 mAh/cm^2 for hG/S-50%; Figure 4d). Nevertheless, returning the current density to a lower value of 0.5 mA/cm^2 largely restored its capacity for the high mass loading hG/S-80% cathode (838 mAh/g_S or 7.8 mAh/cm^2, vs. 779 mAh/g_S or 4.5 mAh/cm^2 for hG/S-50%; Figures 4c & d), suggesting the high S content electrode retained its relatively stable high performance at lower currents despite inferior rate capability.

Further increase of S mass loading was achieved by simply adding more powder mixture into the compression die. For example, a high m_{A-S} of 13.9 mg/cm^2 of hG/S-80% was obtained by using 30 mg of the powder mixture. However, numerous measurement results suggest that increasing the S mass loading to >10 mg/cm^2 with S content >70 wt% produced freestanding homogeneous electrodes (with Al current collector) that often exhibited poor S utilization and rechargeability, a general phenomenon for high mass loading, high S content cathodes from various other fabrication techniques.[6] For example, the above hG/S-80% cathode with m_{A-S} = 13.9 mg/cm^2 exhibited a first discharge capacity of only 380 mAh/g_S (or 5.3 mAh/cm^2) and cannot be fully recharged (i.e., no full

conversion back to S). This may be attributed to the increasingly more sluggish electrochemical reaction kinetics with thicker electrodes that have significantly reduced conductivity at high S contents (Figure S10).

2.4. Layered Electrode Architecture Design for High S Content hG/S Cathodes

It was reported that the use of three-dimensional (3D) current collectors such as nickel (Ni) foam would improve slurry-based S cathode performance with improved electrical contacts.[6,43] Ni foam current collectors are compatible with the dry-press technique with the hG/S composite powders of various hG:S ratios. Upon dry compression of the composite powder onto a precisely cut Ni foam disc (Figure S11), it was found that the hG/S mixtures were firmly attached to the Ni foam, providing much improved interfacial contact in comparison to the use of flat Al foil current collectors. The use of Ni foam significantly helped the S utilization at high S contents. For example, at the same current density of 0.5 mA/cm^2, hG/S-80% ($m_{A\text{-}S}$ = 13.9 mg/cm^2) and hG/S-90% ($m_{A\text{-}S}$ = 15.6 mg/cm^2) discs pressed onto Ni foam exhibited first discharge capacities of 1225 and 1144 mAh/g$_S$ (or 16.3 and 17.2 mAh/cm^2), respectively, while that of the Al foil-supported counterpart was only 380 and 262 mAh/g$_S$ (or 5.1 and 3.9 mAh/cm^2), respectively.

However, commercially available Ni foam is generally much heavier (35.5 mg/cm^2 in this work) than Al foil (4.3 mg/cm^2 in this work), which would significantly reduce the overall device energy density. Various lightweight foams such as Al, carbon nanotubes, and graphene have been used for weight reduction.[6] However, S incorporation onto these lightweight current collectors often requires slurry casting with the use of a solvent and a binder, or melt infiltration, which requires high temperature but with less control on the S loading.

Dry compressible hG enables a unique lightweight solution for electrode engineering with facile and precise controls of electrode mass loading, composition, and architecture. For example, we previously demonstrated that hG could be readily used as a dry-pressible matrix for facile preparation of high performance, high mass loading air cathodes with layered architectures containing catalysts for Li-O_2 batteries.[41] With a similar layered architectural concept, herein a thin layer of small amount of hG was inserted between the Al current collector and the hG/S active composite layer. It is anticipated that the high S content layer would readily infiltrate into the porous and conductive neat hG "interlayer", which serves as an ultralightweight mimic for foam-like current collectors discussed above. The concept of layered or structured S placement has been previously explored,[44–46] but the dry compression fabrication method used in this work offers much more convenience and freedom in the electrode architectural design.

In a typical facile process to prepare an architectural cathode with a hG interlayer, a piece of Al foil, a small amount of (e.g. 5 mg, or ~2.9 mg/cm^2) neat hG powder, and a desirable amount of hG/S composite powder were sequentially added to the compression die. The composite electrode was then formed after dry-press for ~10 min. As shown in the cross-sectional overlaid SEM/EDS image in Figure 5a, the Al foil and the hG interlayer are tightly associated, suggesting good electrical contact. Impressively, the S signal intensity linescan across the interface suggests that S infiltrated all the way to reach the Al-hG interface, with the intensity approximately 1/5 of that in the main hG/S composite layer. The S signal intensity then gradually increased from that interface through the entire interlayer into the main hG/S layer (hG/S-90% powder was used in this example). Such a smooth transition was made possible by the lightweight nature of both hG and hG/S powder, which intimately inter-infiltrated during the dry compression. The S concentration gradient would likely impart a gradual increase of conductivity toward the current collector, in contrast to a rather abrupt conductivity change at the interface when no hG interlayer was used. Therefore, the hG interlayer effectively functions as an ultralightweight 3D foam-like current collector.

With a large amount of hG/S composite for high S mass loading, the total S content remained high despite the weight of the hG interlayer. For example, a 20 mg hG/S-80% cathode with a 5 mg hG interlayer had a total S content of 64% ("Layered-hG/S-64%") with $m_{A\text{-}S}$ of 9.2 mg/cm^2, while a 30 mg hG/S-90% cathode with a 5 mg hG interlayer had a total S content of 77% ("Layered-hG/S-77%") with $m_{A\text{-}S}$ of 15.6 mg/cm^2. The total cathode densities of these layered hG/S composite cathodes remained high, with the above two cathodes exhibiting densities of 1.14 and 1.45 g/cm^3, respectively.

The use of a hG interlayer significantly improved the performances of high mass loading, high S content S cathodes. As shown in Figure 5b, in comparison to a hG/S-80% cathode with no hG interlayer ($m_{A\text{-}S}$ = 9.2 mg/cm^2; the same one shown in Figure 4b), a cathode made from the same amount of hG/S-80% mixture but with an extra hG interlayer mentioned above (Layered-hG/S-64%) exhibited not only improved S utilization in terms of specific capacity (1370 vs.1291 mAh/g$_S$) and areal capacity (12.7 vs. 11.9 mAh/cm^2), but also much reduced overpotential (ΔE ~ 0.17 vs. 0.49 V). The latter is an unambiguous indication of significantly increased electrochemical reaction kinetics. As shown in Figures 5c & d, the rate performance of this layered cathode also improved significantly from the one without interlayer, with capacity values of 1215, 879, and 402 mAh/g$_S$ (or 10.5, 7.6, and 3.5 mAh/cm^2) at current densities of 1, 2, and 5 mA/cm^2, respectively, while those for the non-layered hG/S-80% electrode with the same 9.2 mg/cm^2 mass loading were only 184, 117, and 30 mAh/g$_S$ (or 1.7, 1.1, and 0.3 mAh/cm^2), respectively. As also shown in Figures 5b-d, the Layered-hG/S-77% cathode with $m_{A\text{-}S}$ as high as 15.6 mg/cm^2 mentioned above also exhibited impressive high capacity of 1270 mAh/g$_S$ (or 19.8 mAh/cm^2, 1418 mAh/cm^3), equivalent to 76% S utilization, with a low overpotential of 0.22 V at 0.5 mA/cm^2. The volumetric capacity is the highest reported thus far at such high S mass loading level (> 9 mg/cm^2 solid S) (Table S1 and Figure S4). It retained a capacity of 503 mAh/g$_S$ (or 7.8 mAh/cm^2, 562 mAh/cm^3) at 1 mA/cm^2. Despite expected reduced performance with increasing current, the battery

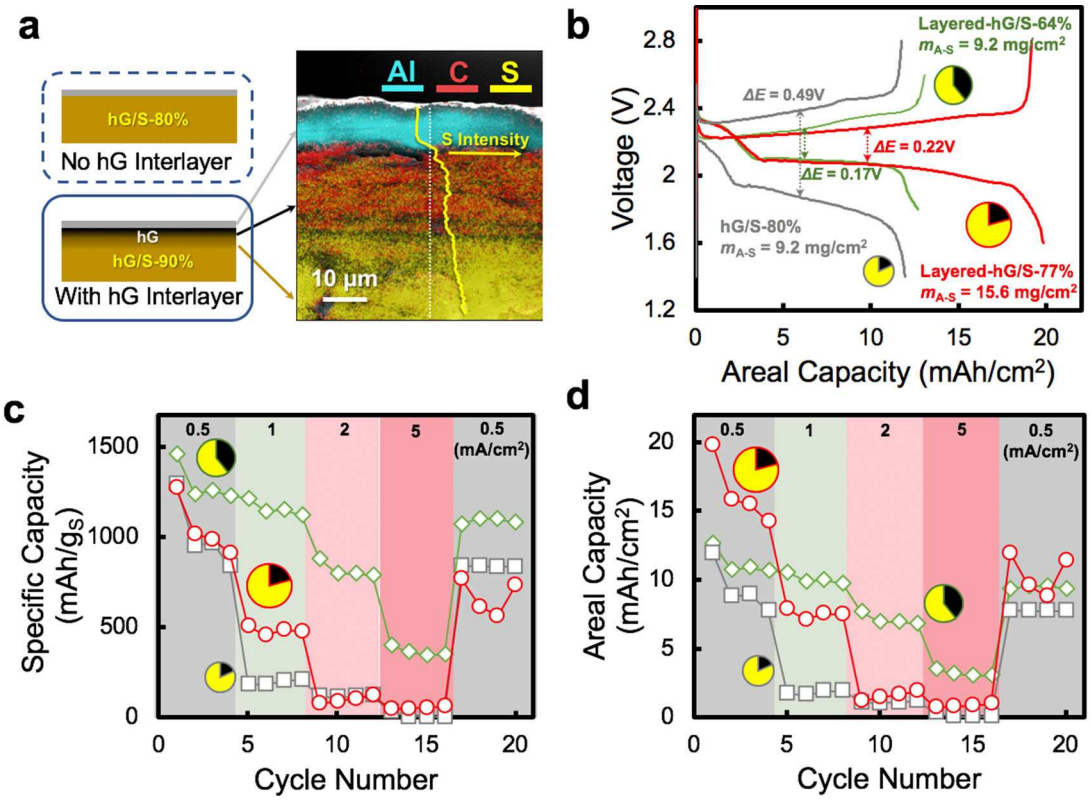

Figure 5. a) Schematic illustration and the corresponding typical overlaid cross-sectional SEM/EDS image of a hG/S composite cathode with high S mass loading (15.6 mg/cm^2) with the use of a neat hG interlayer (2.9 mg/cm^2). The S content for the hG/S layer was 90%; therefore, the total S content considering the hG interlayer was 77%. The EDS linescan of the S signal corresponding to the dashed line is also overlaid in the image. b) The first cycles of Li–S batteries with various cathodes: hG/S-80% with no interlayer ($m_{A\text{-}S}$ = 9.2 mg/cm^2), Layered-hG/S-64% ($m_{A\text{-}S}$ = 9.2 mg/cm^2), and Layered-hG/S-77% ($m_{A\text{-}S}$ = 15.6 mg/cm^2). c) and d) are the rate performances of the same cathodes in terms of specific and areal capacity values, respectively. The inset symbols in each of the b)-d) panels indicate the S content in the cathodes (yellow: S; black: hG).

capacity was restored back to 766 mAh/g_S (or 12.0 mAh/cm^2, 855 mAh/cm^3) after returning the current density back to 0.5 mA/cm^2.

Like most other S cathodes with comparably high mass loading and S content from various approaches reported in the literature,[2–4] the dry-pressed hG/S cathodes, despite the use of hG interlayer, generally exhibited a relatively high capacity fading rate and moderate cyclability (< 50 cycles). As shown in the post mortem analyses in the previous section, the cycled cathode exhibited much reduced structural integrity and the cycled Li anode surface was significantly degraded. A major cause for the performance and structural degradation can be attributed to the dissolution and shuttling of polysulfide intermediate species.[2–6] While hG as a porous carbon material may serve as a polysulfide adsorbent, no further specific management was conducted to prevent S loss from the shuttling effect in the current work, as it was a first concept demonstration for the fabrication of dry-pressed S composite cathodes. Nevertheless, various methods can be envisioned to further improve cyclability. For example, with regard to cathode modification, heteroatomic doping of the hG[14,15]or the use of certain transition metal oxide nanoparticles (e.g., TiO_2,[17] MnO_2,[47] etc.) are viable approaches to reduce polysulfide shuttling. In addition, protected separator membranes have also been extensively explored in the literature[6,48] and can be similarly applied with Li–S batteries using the dry-pressed hG/S cathodes. The use of appropriate electrolyte is also critical to the cycling performance of Li–S batteries.[49] Applications of gel polymer[50] or ceramic[51] solid-state electrolytes, as well as liquid electrolytes that exhibit low polysulfide solubility,[52] are also attractive strategies to reduce polysulfide shuttling and improve cyclability. These studies are currently underway in our laboratories.

3. Conclusions

A highly facile, solvent-free and binder-free process enabled by the use of holey graphene as a dry-pressible cathode scaffold host is reported for the fabrication of high mass loading, high S content composite cathodes that exhibit outstanding properties in terms of gravimetric, areal, and volumetric performance. The entire fabrication process, including powder mixing and electrode formation via dry compression, only take a few minutes, in comparison to the lengthy conventional slurry-based casting process that often uses toxic organic solvents and parasitic polymer binders. Since the duration of compression is independent of the electrode mass loading, this process is especially amenable for high mass loading electrodes, which often pose a challenge for solvent-based or melt infiltration

methods in terms of fabrication time and/or loading controllability. The process also enables the convenient manipulation of electrode architecture. For example, the use of a hG interlayer between the Al current collector and the main S-containing composite body significantly improves the S utilization and rate performance of high mass loading, high S content cathodes. The reduced fabrication time and added flexibility in S mass loading and architectural manipulation makes the dry-press approach using the hG scaffold host an attractive option for further scale-up toward commercialization.

Experimental Section

Materials

Graphene powder (Vor-X; grade: reduced 070; lot: BK-77x) was provided by Vorbeck Materials. Holey graphene (hG) was prepared from graphene using the established facile one-step air oxidation procedure published elsewhere.[33,34,39–41] Bis(trifluoromethane)sulfonimide lithium salt (LiTFSI; 99.95%), lithium nitrate ($LiNO_3$; 99.99%), 1,2-dimethoxyethane (DME; anhydrous, 99.5%), 1,3-dioxolane (DOL; anhydrous, 99.8%) were purchased from Aldrich. Lithium chips (15.6 mm diameter, 0.45 mm thickness), Celgard membrane (0.025 mm thickness), aluminum (Al) foil (0.015 mm thickness), and nickel (Ni) foam (1.6 mm thickness) were purchased from MTI Corporation. All chemicals for batteries were handled inside an Ar-filled glovebox with O_2 and H_2O contents <1 ppm. Solvents were dried over freshly regenerated molecular sieves before use. All other materials and chemicals were used as-received.

hG/S Powder Mixture

In a typical experiment, 100 mg hG and a desirable amount of S powder (100, 400, or 900 mg for weight ratios of 1:1, 1:4, or 1:9) were loaded in a 20-mL zirconia vial (SPEX CertiPrep, 6.4 cm long, 5.7 cm outer diameter). After placing two zirconia balls (SPEX CertiPrep, $d=1.3$ cm) in the vial, the set was secured in a SPEX CertiPrep 8000D High-Energy Shaker Mill and subject to mechanical shaking (~1060 back-and-forth cycles per minute, 5.7 cm back-and-forth and 2.5 cm side-to-side movements) for 10 seconds to yield the hG/S powder mixture.

hG/S Composite Cathodes

In a typical experiment to prepare a hG/S composite cathode, a desirable amount of as-prepared hG/S powder mixture was loaded into a stainless steel pressing die (MTI Corporation; Model EQ-Die-15D; manufacturer identified inner diameter 14.85 mm). The assembly was then placed in a hydraulic press (Carver Hydraulic Unit Model #3925) and a load of ~200 MPa was applied for ~10 minutes. The completed disc with typical area of 1.73 cm^2 was readily removed from the die and directly used as the composite cathode for Li–S batteries in the form of CR2032 coin cells. During the sample loading, two pieces of precisely cut (15 mm in diameter) Celgard membrane or Al foil discs were often used as separation layers to prevent unwanted material adhesion to both upper and lower inner die surfaces. Freestanding electrode discs were formed by peeling off both upper and lower separation layers. For most electrodes investigated in this work, one Al disc was left attached to serve as the current collector. For electrodes with a layered architecture, the desirable amounts of components were placed sequentially into the die and subjected to the same dry-press procedure.

Li-S Battery Coin Cells

Li–S batteries were assembled using typical CR2032 coin cell parts (MTI Corporation) with a hydraulic crimper (MTI Corporation, Model MSK-110) inside an Ar-filled glovebox (MBraun Labmaster 130) with O_2 and H_2O contents <1 ppm. The hG/S composite electrode and a piece of Li chip (15.6 mm in diameter; 0.45 mm in thickness; MTI Corporation, EQ-Lib-LiC45) were used as the cathode and anode respectively, with a 19-mm Celgard membrane as the separator. The electrolyte was 1 M LiTFSI and 0.2 M $LiNO_3$ in DME:DOL (1:1, v/v). The total amount of electrolyte added was either 120 μL or 180 μL for S mass loadings lower or higher than 10 mg/cm^2, respectively. Therefore, for the four different mass loadings reported in this work (6, 9.2, 13.9, 15.6 mg/cm^2), the E/S ratios were 11.6, 7.5, 7.5, and 6.7, respectively.

Measurements

Scanning electron microscopy (SEM) images were acquired using a Hitachi S-5200 field emission SEM (FE-SEM) system at an acceleration voltage of 20 kV. A Rigaku SmartLab X-ray Diffractometer with a Cu Kα radiation source was employed for XRD analyses. Nitrogen adsorption-desorption isotherms and the corresponding BET surface area values and BJH (Barrett–Joyner–Halenda) pore characteristics were acquired on a Quantachrome Nova 2200e Surface Area and Pore Size Analyzer system using a 9-mm bulbless cell. The samples were weighed prior to degassing overnight at 100 °C. Battery discharge/charge measurements were conducted on a BST8-MA or a BST8-300-CST 8-Channel Battery Analyzer (MTI Corp.). Current densities used were calculated according to the area of cathode (1.73 cm^2) and range from 0.5–5 mA/cm^2 in this work. Electrochemical impedance spectroscopy (EIS) and cyclic voltammetry (CV) were conducted on a BioLogic VMP-3 electrochemical station. EIS was measured at the open circuit potential in the frequency range of 1 MHz to 0.01 Hz with an amplitude of 10 mV and 10 points measured per decade. CV was scanned in the voltage range of 1.6–2.6 V at a scan rate of 0.01 mV/s.

Acknowledgements

We thank C. Plaza-Rivera for experimental assistance. Financial supports from the NASA Langley Internal Research and Development (IRAD) Program and Convergent Aeronautics Solutions (CAS) Incubation Award are gratefully acknowledged. K. Jones and L. Greenburg were NASA Interns, Fellows, and Scholars (NIFS) Program interns supported by IRAD and CAS Incubation Award, respectively.

Conflict of Interest

The authors declare no conflict of interest.

Keywords: lithium-sulfur batteries · holey graphene · high mass loading · solvent-free · volumetric capacity

[1] P. G. Bruce, S. A. Freunberger, L. J. Hardwick, J.-M. Tarascon, *Nat. Mater.* **2012**, *11*, 19.
[2] A. Manthiram, Y. Fu, S.-H. Chung, C. Zu, Y.-S. Su, *Chem. Rev.* **2014**, *114*, 11751.
[3] Y.-X. Yin, S. Xin, Y.-G. Guo, L.-J. Wan, *Angew. Chem. Int. Ed.* **2013**, *52*, 13186.
[4] Q. Pang, X. Liang, C. Y. Kwok, L. F. Nazar, *Nat. Energy* **2016**, *1*, 16132.
[5] Z. W. Seh, Y. Sun, Q. Zhang, Y. Cui, *Chem. Soc. Rev.* **2016**, *45*, 5605.
[6] H.-J. Peng, J.-Q. Huang, X.-B. Cheng, Q. Zhang, *Adv. Energy Mater.* **2017**, *7*, 1700260.
[7] X. Ji, K. T. Lee, L. F. Nazar, *Nat. Mater.* **2009**, *8*, 500.
[8] L. Yuan, H. Yuan, X. Qiu, L. Chen, W. Zhu, *J. Power Sources* **2009**, *189*, 1141.
[9] J. Guo, Y. Xu, C. Wang, *Nano Lett.* **2011**, *11*, 4288.
[10] Z. Yuan, H.-J. Peng, J.-Q. Huang, X.-Y. Liu, D.-W. Wang, X.-B. Cheng, Q. Zhang, *Adv. Funct. Mater.* **2014**, *24*, 6105.
[11] H. Wang, Y. Yang, Y. Liang, J. T. Robinson, Y. Li, A. Jackson, Y. Cui, H. Dai, *Nano Lett.* **2011**, *11*, 2644.
[12] L. Ji, M. Rao, H. Zheng, L. Zhang, Y. Li, W. Duan, J. Guo, E. J. Cairns, Y. Zhang, *J. Am. Chem. Soc.* **2011**, *133*, 18522.
[13] G. Zhou, L. Li, C. Ma, S. Wang, Y. Shi, N. Koratkar, W. Ren, F. Li, H.-M. Cheng, *Nano Energy* **2015**, *11*, 356.
[14] Y. Qiu, W. Li, W. Zhao, G. Li, Y. Hou, M. Liu, L. Zhou, F. Ye, H. Li, Z. Wei, S. Yang, W. Duan, Y. Ye, J. Guo, Y. Zhang, *Nano Lett.* **2014**, *14*, 4821.
[15] C. Tang, Q. Zhang, M.-Q. Zhao, J.-Q. Huang, X.-B. Cheng, G.-L. Tian, H.-J. Peng, F. Wei, *Adv. Mater.* **2014**, *26*, 6100.
[16] M.-K. Song, Y. Zhang, E. J. Cairns, *Nano Lett.* **2013**, *13*, 5891.
[17] Z. Xiao, Z. Yang, L. Wang, H. Nie, M. Zhong, Q. Lai, X. Xu, L. Zhang, S. Huang, *Adv. Mater.* **2015**, *27*, 2891.
[18] H. Shi, W. Lv. C. Zhang, D.-W. Wang, G. Ling, Y. He, F. Kang, Q.-H. Yang, *Adv. Funct. Mater.* **2018**, *28*, 1800508.
[19] M. Hagen, D. Hanselmann, K. Ahlbrecht, R. Maça, D. Gerber, J. Tübke, *Adv. Energy Mater.* **2015**, *5*, 1401986.
[20] J. Xiao, *Adv. Energy Mater.* **2015**, *5*, 1501102.
[21] J. Song, T. Xu, M. L. Gordin, P. Zhu, D. Lv, Y. B. Jiang, Y. Chen, Y. Duan, D. Wang, *Adv. Funct. Mater.* **2014**, *24*, 1243.
[22] S.-H. Chung, C.-H. Chang, A. Manthiram, *Adv. Funct. Mater.* **2018**, *28*, 1801188.
[23] M.-K. Song, S. Park, F. M. Alamgir, J. Cho, M. Liu, *Mater. Sci. Eng. R* **2011**, *72*, 203.
[24] M. A. Pope, I. A. Aksay, *Adv. Energy Mater.* **2015**, *5*, 1500124.
[25] D. Lv, J. Zheng, Q. Li, X. Xie, S. Ferrara, Z. Nie, L. B. Mehdi, N. D. Browning, J. Zhang, G. L. Graff, J. Liu, J. Xiao, *Adv. Energy Mater.* **2015**, *5*, 1402290.
[26] Y. Ma, H. Zhang, B. Wu, M. Wang, X. Li, H. Zhang, *Sci. Rep.* **2015**, *5*, 14949.
[27] F. Zeng, A. Wang, W. Wang, Z. Jin, Y.-S. Yang, *J. Mater. Chem. A* **2017**, *5*, 12879.
[28] H. M. Kim, H.-H. Sun, I. Belharouak, A. Manthiram, Y.-K. Sun, *ACS Energy Lett.* **2016**, *1*, 136.
[29] Y. Lin, Y. Liao, Z. Chen, J. W. Connell, *Mater. Res. Lett.* **2017**, *5*, 209.
[30] X. Zhao, C. M. Hayner, M. C. Kung, H. H. Kung, *ACS Nano* **2011**, *5*, 8739.
[31] Y. Lin, J.-W. Kim, D. W. Baggett, D. W. Working, J. W. Connell, *Nanoscale* **2013**, *5*, 7814.
[32] J. G. Radich, P. V. Kamat, *ACS Nano* **2013**, *7*, 5546.
[33] X. Han, M. R. Funk, F. Shen, Y.-C. Chen, Y. Li, C. J. Campbell, J. Dai, X. Yang, J.-W. Kim, Y. Liao, J. W. Connell, V. Barone, Z. Chen, Y. Lin, L. Hu, *ACS Nano* **2014**, *8*, 8255.
[34] Y. Lin, X. Han, C. J. Campbell, J.-W. Kim, B. Zhao, W. Luo, J. Dai, L. Hu, J. W. Connell, *Adv. Funct. Mater.* **2015**, *25*, 2920.
[35] Y. Xu, Z. Lin, X. Zhong, X. Huang, N. O. Weiss, Y. Huang, X. Duan, *Nat. Commun.* **2014**, *5*, 4554.
[36] Y. Zhao, C. Hu, L. Song, L. Wang, G. Shi, L. Dai, L. Qu, *Energy Environ. Sci.* **2014**, *7*, 1913.
[37] M. Patel, W. Feng, K. Savaram, M. R. Khoshi, R. Huang, J. Sun, E. Rabie, C. Flach, R. Mendelsohn, E. Garfunkel, H. He, *Small* **2015**, *11*, 3358.
[38] X. Han, Z. Yang, B. Zhao, S. Zhu, L. Zhou, J. Dai, J.-W. Kim, B. Liu, J. W. Connell, T. Li, B. Yang, Y. Lin, L. Hu, *ACS Nano* **2017**, *11*, 3189.
[39] E. D. Walsh, X. Han, S. D. Lacey, J.-W. Kim, J. W. Connell, L. Hu, Y. Lin, *ACS Appl. Mater. Interfaces* **2016**, *8*, 29478.
[40] Y. Lin, B. Moitoso, C. Martinez-Martinez, E. D. Walsh, S. D. Lacey, J.-W. Kim, L. Dai, L. Hu, J. W. Connell, *Nano Lett.* **2017**, *17*, 3252.
[41] S. D. Lacey, E. D. Walsh, E. Hitz, J. Dai, J. W. Connell, L. Hu, Y. Lin, *Nano Energy* **2017**, *31*, 386.
[42] Y. Lin, K. A. Watson, S. Ghose, J. G. Smith, T. V. Williams, R. E. Crooks, W. Cao, J. W. Connell, *J. Phys. Chem. C* **2009**, *113*, 14858.
[43] S.-H. Chung, A. Manthiram, *Electrochim. Acta* **2013**, *107*, 569.
[44] Y. Cao, X. Li, I. A. Aksay, J. Lemmon, Z. Nie, Z. Yang, J. Liu, *Phys. Chem. Chem. Phys.* **2011**, *13*, 7660.
[45] G. Zhou, S. Pei, L. Li, D.-W. Wang, S. Wang, K. Huang, L.-C. Yin, F. Li, H.-M. Cheng, *Adv. Mater.* **2013**, *26*, 625.
[46] L. Luo, A. Manthiram, *ACS Energy Lett.* **2017**, *2*, 2205.
[47] Z. Li, J. Zhang, X. W. Lou, *Angew. Chem. Int. Ed.* **2015**, *54*, 12886.
[48] J. Q. Huang, Q. Zhang, F. Wei, *Energy Storage Mater.* **2015**, *1*, 127.
[49] S. Zhang, K. Ueno, K. Dokko, M. Watanabe, *Adv. Energy Mater.* **2015**, *5*, 1500117.
[50] M. Liu, D. Zhou, Y. B. He, Y. Fu, X. Qin, C. Miao, H. Du, B. Li, Q.-H. Yang, Z. Lin, T. S. Zhao, F. Kang, *Nano Energy* **2016**, *22*, 278.
[51] K. Fu, Y. Gong, G. T. Hitz, D. W. McOwen, Y. Li, S. Xu, Y. Wen, L. Zhang, C. Wang, G. Pastel, J. Dai, B. Liu, H. Xie, Y. Yao, E. D. Wachsman, L. Hu, *Energy Environ. Sci.* **2017**, *10*, 1568.
[52] N. Azimi, Z. Xue, I. Bloom, M. L. Gordin, D. Wang, T. Daniel, C. Takoudis, Z. Zhang, *ACS Appl. Mater. Interfaces* **2015**, *7*, 9169.

Manuscript received: April 9, 2019
Revised manuscript received: May 24, 2019
Version of record online: June 18, 2019